Analysis of Hydration Kinetics of Lithium Carbonate-Oil Well Cement at 4 ℃—Application to Cementing of Natural Gas Hydrate Layer

Chengquan Li[1,a], Bo Liu[1,b], Chaoping Zhang[1,c], Zhaocai Yu[1,d], Tianan Deng[1,e], Huanjie Liu[1,f], Xiaohui Yang[1,g], Jingxuan Cai[2,3,*]

[1]PetroChina Southwest oil and gas field development division, Chengdu, 610066, China
[2]School of New Energy and Materials, Southwest Petroleum University, Chengdu, 610500, China
[3]State Key Laboratory of Oil & Gas Reservoir Geology and Exploitation, Southwest Petroleum University, Chengdu, 610500, China

[a]lichengq@petrochina.com.cn, [b]liubo08@petrochina.com.cn, [c]zhangchaop@petrochina.com.cn, [d]yuzhaocai@petrochina.com.cn [e]dengtiana223@petrochina.com.cn, [f]liuhjxx@petrochina.com.cn [g]yangxiaoh447@petrochina.com.cn
*Corresponding author Jingxuan Cai: 724544183@qq.com

Abstract. It is common for cement pastes to require high early strength when cementing in unusual locations, such as deepwater, ultra-deepwater, or cold polar seas. While prior research indicates that lithium salts may substantially enhance the early strength of cement pastes, the effect of TSL on the hydration process of oil well cement remains ambiguous. This study examined the effect of TSL on the hydration of Class G oil well cement at low temperatures by kinetic and microstructural evolution investigations. The study revealed that TSL enhances the extent of cement hydration and optimizes the hydration effects during the NG, I, and D phases of hydration. A superficial layer of calcium carbonate (Cc) hydration products enhanced the mechanical characteristics of cement pastes by facilitating the orderly growth of ettringite (AFt) and calcium hydroxide (CH) hydration products, as well as promoting the interlocking and densification of the spatial structure of hydrated calcium silicate (C-S-H). The compressive strength of cement pastes after 48 hours at a curing temperature of 4 ℃ is 14.49 ± 0.31 MPa, meeting the requirements for cementing construction, when a TSL dosage of 4% is used. As a result, TSL has the potential to act as a low-temperature early-strengthening agent for Class G oil well cement, providing a theoretical and experimental foundation for addressing the issue of inadequate cement strength development and for developing early-strengthening cementing slurries for unconventional regions like deep water, ultra-deep water, and the polar cold sea.

Keywords: low temperature environment, cementing slurry, lithium carbonate, hydration kinetics, hydration mechanism.

H. Bilgin et al. (eds.), *Proceedings of the 2024 6th International Conference on Civil Engineering, Environment Resources and Energy Materials (CCESEM 2024)*, Advances in Engineering Research 253,
https://doi.org/10.2991/978-94-6463-606-2_31

1 Introduction

The comprehensive exploration and exploitation of oil and gas resources have rendered unconventional environments, such as deepwater, ultra-deepwater, and polar cold seas, increasingly vital as strategic alternatives to conventional oil and gas resources [1-3]. However, their special geological environment, such as loose formations, the presence of shallow water-air currents and low temperature environments, pose a great challenge to cementing technology [4-6]. The need to minimise the cementing time in unconventional areas requires cement pastes with excellent early strength. The main challenge for cementing in these areas is the low temperature [7], which is only about 4°C at the seabed mudline and can be as low as -5 to -30 °C in polar regions [8, 9]. The early strength development of conventional cement for cementing is slow or even stops hydration in the low temperature environment [10], which not only increases the cost of oil and gas well development, seriously affects the quality of cementing, but also poses major safety hazards [11]. Thus, the development and execution of an early-strength cement slurry system designed for low-temperature cementing, alongside the improvement of early-strength cement pastes to meet the requirements of unconventional cementing, are essential for promoting the safe and efficient extraction of oil and gas resources. The primary technique for enhancing the early strength development of oil well cement pastes involves the incorporation of early-strength promoters into the cement slurry [12, 13]. A variety of early-strength enhancers for oil well cement can be categorized into soluble inorganic salts, soluble organic compounds, nanomaterials, and other classifications [14-16]. Among them, inorganic salts of early strength agents are mainly composed of chloride salts, sulfates, nitrates, alkali metal salts, etc. [17]. Currently more widely used for the chlorinated salts such as calcium chloride, but the incorporation of calcium chloride usually causes the deterioration of the performance of the cement slurry, prone to flash-setting and other phenomena. In addition, precipitation of chloride ions may cause corrosion of the casing. Sulfate-based early-strength accelerators are usually susceptible to alkali aggregate reactions, resulting in deterioration of cement pastes properties. Organic salt early strength agents primarily consist of triethanolamine and triisopropanolamine, among others [18], but the dosage of these early strength accelerators is extremely sensitive and difficult to achieve large-scale practical applications. Nanomaterials class of early-strengthening agent effect is limited, and the dosage requirements are extremely strict, the dosage is too low to cause poor coagulation effect, while the dosage is too high is easy to cause the consistency of the cement paste to become larger and lose fluidity [19, 20]. In addition, nanomaterial-based early-strengthening agents are usually more expensive. With the increasing demands on the performance of cement slurry, multi-component pro-cementing and early-strengthening agents have been increasingly applied and developed [21, 22].

In recent years, some new types of alkali metal chloride early strength agents have been applied in oil well cement, such as sodium chloride, potassium chloride, etc. [23-26], which have shown better promoting and strengthening effects. In addition, lithium alkali metal salts have also been shown to have better promoting and strengthening effects [27], but the study of lithium salts is still limited to chloride and sulphate salts. Mitigating the detrimental effects of chloride and sulfate ions is tough. Consequently,

to mitigate the adverse impacts of chloride and sulfate ions on cement, lithium carbonate (TSL) may serve as a potential early-strengthening accelerator. Previous studies on TSL have mostly focused on its battery performance and catalytic influence on aluminate and sulfoaluminate cement [28-30]. Investigations on the mechanism of early strength augmentation of oil well cement by TSL at low temperatures remain relatively scarce and need a thorough and systematic examination.

This study examined the influence of TSL on the thermokinetic procedure for low-temperature hydration of oil well cement, utilizing Knudsen's extrapolation equation and the Krstulovic-Dabic kinetic model of the hydration reaction. The techniques of X-ray diffraction (XRD), thermogravimetric analysis (TG/DTG), and scanning electron microscopy (SEM) were employed to examine the evolution of TSL on the microstructure of low-temperature cement hydration products. The impact of TSL on the initial compressive strength of Class G oil well cement at 4 ℃ was analyzed, and the micromechanism via which TSL improves the early strength of oil well cement was clarified. To provide particular data and a theoretical framework for addressing the problem of insufficient early strength development in cement pastes during low-temperature cementing.

2 Experiments

2.1 Experimental Materials

The TSL used for the study was supplied by Wuhan Canos Technology Co., Ltd., whilst the Class G oil well cement was sourced from Jahua Special Cement Co., Ltd. and adhered to the API 10A specification. The principal chemical composition is indicated in Table 1. Henan Weihui Chemical Co., Ltd. supplied the water loss reducer (G33S), dispersion (USZ), and defoamer.

Table 1. Chemical composition of Class G oil well cement

Composition (wt. %)	CaO	SiO2	Al2O3	Fe2O3	MgO	Others	Loss
Class G oil well cement	61.79	20.38	3.37	4.15	1.95	5.07	2.61

2.2 Experimental and Characterization Methods

Nine sets of cement slurry specimens were created, maintaining consistent proportions of various admixtures and additives to enhance the visualization of TSL-cement composite performance. The amounts of admixtures and TSL in the preparation of cement slurries were established as a mass percentage of the total dry cement powder, with the dosage of each component detailed in Table 2. Cement slurry with a water-to-cement ratio of 0.44 was created in line with the American Petroleum Institute Recommended Standard for Oil Well Cement Testing (API RP 10B-2-2013). [31]. To prepare the cement slurry, the cement and admixture were first thoroughly mixed in a dry state; if dry mixing was impractical, the admixture was added to the slurry cup and stirred at a low speed of 4000±200 r/min. The well blended mixture was thereafter placed into the

slurry cup within 15 seconds and agitated for 35 seconds ± 1 second at high velocity (12000 ± 500 r/min).

Table 2. Cement slurry formulations

Group	Class G oil well cement(g)	G33S (g)	USZ (g)	TSL (g)	Defoamer(g)	water (g)
G	400	4	2	0	0.2	176
G-1TSL	400	4	2	4	0.0	176
G-2TSL	400	4	2	8	0.2	176
G-3TSL	400	4	2	12	0.2	176
G-4TSL	400	4	2	16	0.2	176
G-5TSL	400	4	2	20	0.2	176
G-6TSL	400	4	2	24	0.2	176
G-7TSL	400	4	2	28	0.2	176
G-8TSL	400	4	2	32	0.2	176

2.2.1 Cement Hydration Heat Test.

The semi-adiabatic method and isothermal calorimetry were utilized to assess the temperature of hydration of cement. The semi-adiabatic technique evaluates the exothermic heat of cement hydration utilizing the laboratory's hydration heat testing equipment, in accordance with China's national standard for cement hydration heat testing (GB/T 12959-2008). The calorimeter's loss of heat coefficient in the apparatus is inferior to the international norm of 167 J/(h·°C), tested at a temperature of 4 °C during a period of 72 hours. An eight-channel standard volumetric isothermal heat conductivity calorimeter (TAM Air, TAM Corporation, USA) was utilized to conduct isothermal calorimetry for quantifying the exothermic temperature of hydration of cement. The test lasted approximately 168 hours.

2.2.2 Characterization of Cement Pastes Microstructure.

A DX-2700 X-ray diffractometer produced by Dandong Fangyuan Instrument Co., Ltd. was employed to qualitatively evaluate the alterations in the composition of the physical phase during cement hydration, utilizing a scanning step length of 0.04°, a duration of 1 second per step, and a diffraction angle range of 5-80°. The thermal loss of the cement paste was simultaneously evaluated using a TGA/SDTA851/e thermal analyzer from Mettler Toledo, Switzerland, to ascertain the degree of cement hydration and to examine the mechanism of TSL action. The dried cement paste sample was fractured and subsequently manually pulverized with a mortar and pestle until a uniform consistency was achieved. The samples were subsequently positioned in the instrument, and the testing settings were established, with a temperature range of 40 to 1000 °C, a heating rate of 10 °C/min, and a nitrogen flow rate of 60 mL/min.

The morphological characteristics of the cement paste samples were examined with a ZEISS EVO MA15 electron microscopy instrument manufactured by Carl Zeiss, Germany. The dried cement paste specimens were sliced into thin sections, and the block

specimens were affixed to the specimen holders using conductive adhesive. The freshly manufactured specimen slices were coated with gold via ion sputtering prior to analysis in the scanning electron microscope. The voltage at which the device operated was 5 kV, and the emission rate was 10 μA.

2.2.3 Testing of Compressive Strength of Cement Pastes.

The compressive strength of cement pastes was assessed per the API 10B standard using a TYE-300B pressure testing equipment (Wuxi Jianyi Instrument Machinery Co., Ltd.) at a rate of loading of 71.7 kN/min ± 7.2 kN/min. The specimens were cured at the temperature of 4 ℃ for periods of 12 h, 24 h, and 48 h, with dimensions of 50.8 mm × 50.8 mm × 50.8 mm. Each group consisted of five specimens, and the mean value was documented as the end outcome.

3 Results and Discussion

3.1 Cement Hydration Exothermic

Class G oil well cement with 0 % and 4 % TSL underwent 96 hours of semi-adiabatic testing to ascertain the hydration increase in temperature curves and cumulative heat release during hydration. The findings may be seen in Figures 1 and 2. Classes G and H oil well cement with 0 % and 4 % TSL hydration temperature increase curves are shown in Fig. 1. A more rapid and intense hydration reaction in the cement results in a rapid release of a substantial quantity of hydration heat, as seen by the sharper peak of the G-4TSL hydration temperature rise compared to G. The use of TSL reduces the initial stage of cement hydration, since Li^+ accelerates the degradation of the first hydration product coating around the surfaces of cement particles. This, in turn, increases the cement-water contact area, speeds up the hydration reaction, and allows cement hydration to enter the accelerated hydration period earlier. The incorporation of TSL diminishes the induction stage of the cement hydration process, as Li+ promotes the disintegration of the initial hydration product layer encasing cement particles, thereby increasing the contact area between cement and water, accelerating the hydrate reaction, and allowing the cement hydration process to enter the accelerated hydration phase more promptly. During the accelerated hydration phase, the hydration temperature rise rate of G-4TSL increased by 52.70 % relative to G. The peak hydration temperature rise of G-4TSL was increased by 34.29 % compared with that of G. The time of occurrence of the peak of maximum hydration temperature rise was advanced by 36. The maximum hydration temperature rise of G-4TSL was increased by 36.32% from 53.00 h to 33.75 h. During the deceleration period, the hydration temperature rise rate of G-4TSL increased by 38.46 % compared to that of G. The cement hydration then entered a stable period.

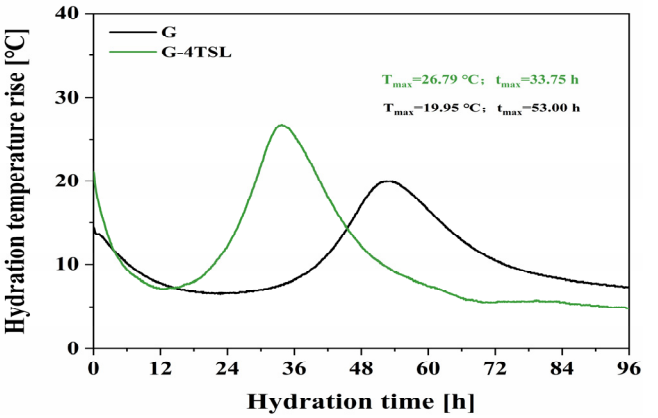

Fig. 1. Cement hydration temperature rise curves of G and G-4TSL

Fig. 2 depicts the cumulative exothermic curves for G and G-4TSL. The cumulative heat emission of G-4TSL hydrated for 12 hours is 11.42 % less than that of G. The cumulative heat release of G-4TSL hydrated for 24 hours is 30.00 % greater than that of G, whereas the cumulative heat production of G-4TSL hydrated for 48 hours is 70.01 % greater than that of G. The cumulative heat emission of G-4TSL hydrated for 72 hours is 3.06 % less than that of G. The use of TSL reduces cumulative heat release in the beginning and end stages of cement hydration, while increasing heat release during the accelerated and decelerated stages. This phenomenon arises as TSL reduces the induction stage of hydration of cement, facilitating an earlier shift into the accelerated phase. Concurrently, it accelerates the rate of hydration processes during the expedited phase of hydration of cement.

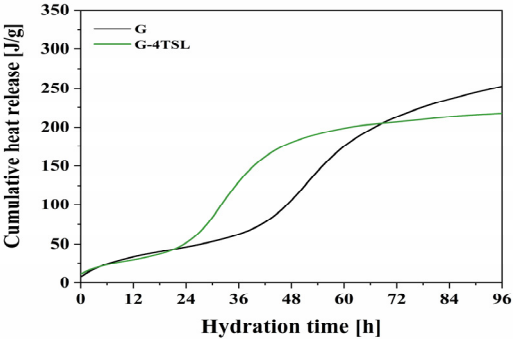

Fig. 2. Cumulative heat release curves of cement hydration of G and G-4TSL

3.2 Hydration Kinetics

3.2.1 Isothermal Calorimetry of Hydration Enthalpy

The influence of TSL on the process of hydration of G was examined by isothermal calorimetry. We measured the cumulative exothermic heat release over 168 hours and

compared the heat flow fluctuations during hydration of G that was either pure or infused with 4% TSL. The test results are depicted in Figs. 3 and 4, respectively. Fig. 3 illustrates that during the first reaction phase, the heat flow of G and G-4TSL escalated swiftly, exhibiting the first peak in heat flow variation, subsequently followed by a quick decline in heat flow values. This phase relates to the exothermic wetness and dissolution of particles of cement, the fast response of the mineral phase C_3A inside the cement, and the heat generated by the synthesis of low-calcium hydration products from certain C_3S components. The maximum initial heat flow of G-4TSL is just 0.0044 W/g, in contrast to the peak initial heat flow of G, which is 0.0146 W/g. The peak heat flow following TSL doping is decreased by 69.86% in comparison to G. This suggests that the presence of TSL may have hindered the rapid reaction of C_3A and the formation of poor calcium hydration products resulting from some C_3S. The induction phase of cement hydration commences when the concentration of reactive ions in the liquid phase of the cement paste diminishes and first hydration products are generated. The thermal flow from G-4TSL during the hydration initiation phase was marginally superior to that of G and commenced the accelerated cement hydration phase sooner. The second peak in heat flow emerged following the beginning of the accelerated cement hydration phase, and this peak was associated with the continued hydration reactions of C_3S and C_2S in the cement. During the accelerated cement hydration phase, the hydration response rate of G-4TSL surpasses that of G. The maximum of the second heat flow for G-4TSL is 0.0030 W/g, but for G it is about 0.0025 W/g. Subsequent to the peak of the second thermal alteration, the heat flow of the cement paste commences to decline, entering the deceleration phase of the cement hydration process, marked by the formation of products of hydration that include C-S-H and CH resulting from the rapid hydration of C_3S. The speed of the hydration process decreases again due to the buildup of various hydration products, cross-linking of these products, reduction of the reaction space among unhydrated cement particles, scarcity of free water, and encapsulation of unhydrated particles of cement by the hydration products. The cement hydration reaction advances to the stabilization phase, during which hydration is mostly controlled by diffusion.

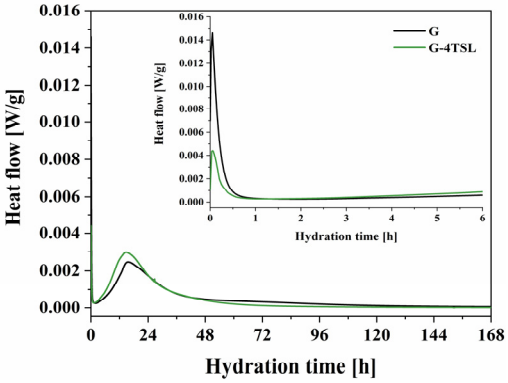

Fig. 3. Heat flow variations during hydration of G and G-4TSL

Fig. 4 illustrates the cumulative heat emission during the hydration of G and G-4TSL over a period of 168 hours. The cumulative heat release from hydration determined with isothermal calorimetry aligns with the cumulative heat release from hydration computed using the semi-adiabatic approach. The cumulative heat output from the hydration of G-4TSL is inferior to that of G throughout both the initial cement hydration phase and the hydration induction phase. Throughout the accelerated hydration phase, the cumulative heat of hydration of G-4TSL escalates swiftly. Following 24 hours of hydration, the cumulative heat of hydration for G-4TSL was 160.43 J/g, whereas for G it was 134.20 J/g. Following 48 hours of hydration, the cumulative heat of hydration for G-4TSL was 235.71 J/g, whereas for G it was 210.77 J/g. The cumulative heat release throughout the hydration of G-4TSL was 255.63 J/g, whereas for G it was 244.57 J/g, measured over a period of 72 hours. The cumulative hydration heat release curve of the cement intersects for the second time at 85.84 hours, with a heat release of 259.50 J/g. Consequently, the total heat emission of G surpasses that of G-4TSL. The discrepancy in timing between this junction point and the intersection point derived from the semi-adiabatic test may be attributed to the variance in TSL solubility.

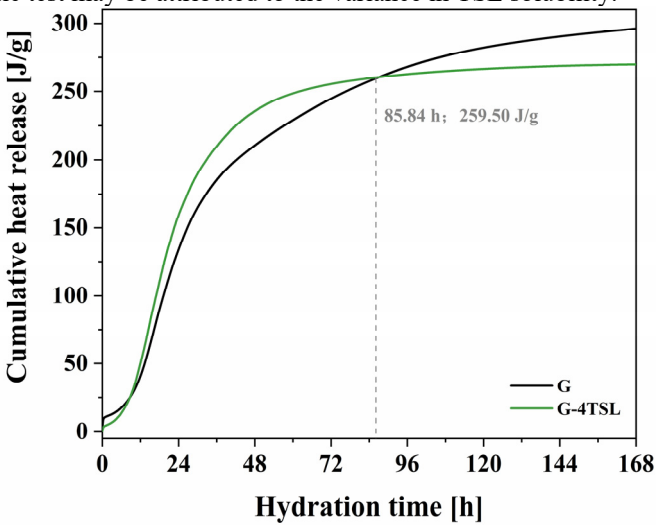

Fig. 4. Cumulative heat release of hydration of G and G-4SL from isothermal calorimetry tests

Through the examination of heat flow variations and the cumulative exothermic change principle during the hydration of G and G-4TSL, the curve depicting the cement hydration exothermic rate over varying hydration durations was computed, as illustrated in Fig. 5. The pattern of the cement hydration exothermic rate curve aligns with the trend of the heat flow alterations. The alteration in the hydration exothermic rate curve of G-4TSL resembles that of G, and the peak morphology of the hydration exothermic rate is analogous, suggesting that the hydration exothermic rate of cement with 4% TSL incorporation remains generally moderate. During the initial phase of cement hydration, the exothermic rate of G was 49.80 J/(g·h), whereas that of G-4TSL was 15.82 J/(g·h), representing a reduction of 68.23 % compared to G. In the accelerated

cement hydration phase, the exothermic hydration rate of G-4TSL was markedly superior to that of G, suggesting that TSL enhances the hydration reaction during this period. This phenomenon is ascribed to the ability of Li^+ in the liquid phase of the cement slurry to interact with OH- to produce LiOH, thereby augmenting the alkalinity of the liquid phase environment. The maximum hydration exotherm rate of G-4TSL was 10.73 J/(g·h) during the accelerated phase, whereas the peak rate for G was just 8.87 J/(g·h), indicating a 20.97 % enhancement following the incorporation of TSL relative to pure Class G oil well cement. In the deceleration and stabilization phases of cement hydration, the exothermic rates of G and G-4TSL were comparable, attributed to the reduction in the concentration of reactive ions in the liquid phase and the substantial quantity of hydration products surrounding the unhydrated cement particles.

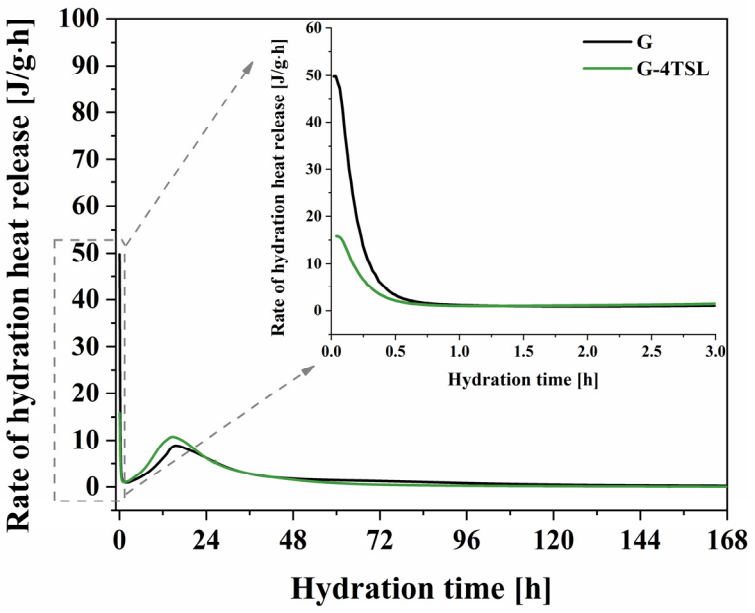

Fig. 5. Exothermic rate of cement hydration for G and G-4SL obtained by isothermal calorimetric testing

α(t) is the basic parameter of hydration kinetics that characterises the degree of hydration of the cementitious materials, which can be calculated from the exotherm of hydration derived by Knudsen, the cumulative exotherm of hydration versus time, as shown in Eqs. (1) and (2) [32]:

$$\alpha(t)=Q(t)/Q_{max} \tag{1}$$

$$\frac{1}{Q}=\frac{1}{Q_{max}}+\frac{t_{50}}{Q_{max}(t-t_0)} \tag{2}$$

Q(t) represents the heat of hydration at the commencement of the accelerated phase of cement hydration, measured in joules (J); Q_{max} denotes the exothermic heat of hydration of the cementitious material at infinite age, also in joules (J); t50 indicates the

duration required for the exothermic heat of cement to attain 50 % of the maximum value Q_{max}, expressed in hours (h); and t_0 signifies the conclusion of the induced phase of cement hydration, marking the onset of the accelerated period, measured in hours (h).

Fig. 6 shows the Q_{max} fitting curves of G and G-4TSL, and Table 3 shows the hydration thermodynamic parameters of G and G-4TSL. From Fig. 6, the Q_{max} fits of G and G-4TSL are higher, and the R^2 reaches 0.99985 and 0.99963, respectively, and the t_{50} fits of G was obtained from the fitted curve, but the t_{50} fits of G-4TSL was worse, which may be related to the mechanism of action of TSL on cement hydration.

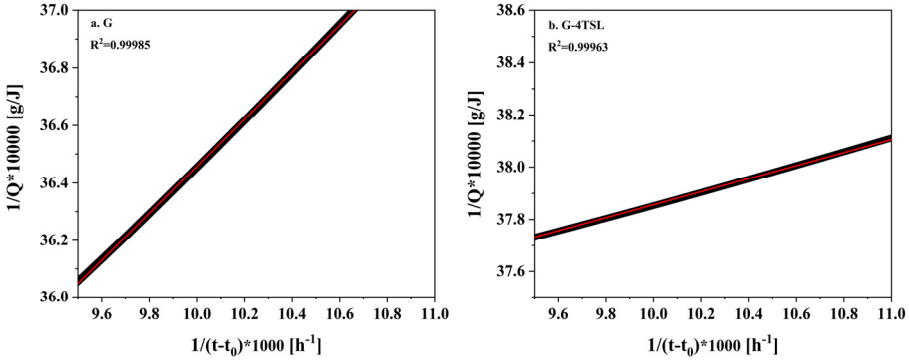

Fig. 6. Plot of Q_{max} fitting curves for G and G-4TSL (a. Q_{max} fitting curve for G, b. Q_{max} fitting curve for G-4TSL)

Table 3. Thermodynamic parameters of G and G-4TSL

Group	Qmax[J/g]	t50[h]	Knudsen equation	Regression factor [R^2]
G	353.36	28.90	1/Q=0.00283+0.0818/(t-t0)	0.99985
G-4TSL	279.33	6.96	1/Q=0.00358+0.0249/(t-t0)	0.99963

3.2.2 Hydration Kinetic Parameters.

The Krstulovic-Dabic kinetic model of the reaction of hydration in cementitious materials categorizes the hydration process of cement into three separate phases: the growth and nucleus formation phase (NG), the interphase interaction phase (I), and the diffusion phase (D). The phases were obtained from the model and the exothermic heat of hydration of the cementitious components was assessed under isothermal circumstances [33]. During the initial phase of cement hydration, the process is primarily governed by the NG mechanism. As the hydration reaction advances, the accumulation of hydration products on the surfaces of the cement particles increases, leading to a reduction in free water content. Consequently, the migration of ionic elements becomes progressively more challenging, with the hydration process transitioning to be predominantly influenced by the I mechanism, and ultimately by the D mechanism. The kinetics of hydration in the cement hydration reaction may be represented by equations (3) to (5) for the aforementioned three stages [34, 35].

[1] Nucleation and growth of crystals, NG

$$[-\ln(1-\alpha)]^{\frac{1}{n}}=K_1(t-t_0)=K_1'(t-t_0) \quad (3)$$

[2] Interphase reaction, I

$$[1-(1-\alpha)^{\frac{1}{3}}]^{1}=K_2r^{-1}(t-t_0)=K_2'(t-t_0) \quad (4)$$

[3] Diffusion, D

$$[1-(1-\alpha)^{\frac{1}{3}}]^{2}=K_3r^{-2}(t-t_0)=K_3'(t-t_0) \quad (5)$$

The differentiation of Equations (3) to (5) produces the kinetic Equations (6) to (8), which specify the hydration speeds of the NG, I, and D operations.

Hydration rate equation for the NG process,

$$d\alpha/dt=F_1(\alpha)=K_1'n(1-\alpha)[-\ln(1-\alpha)]^{(n-1)/n} \quad (6)$$

Hydration rate equation for the I process,

$$d\alpha/dt=F_2(\alpha)=K_2'3(1-\alpha)^{2/3} \quad (7)$$

Hydration rate equation for the D process,

$$d\alpha/dt=F_3(\alpha)=K_3'3(1-\alpha)^{2/3}/[2-2(1-\alpha)^{1/3}] \quad (8)$$

In this context, α denotes the level of hydration, while K_1、K_2、K_3、K_1'、K_2' and K_3' represent the constants of reaction rate for the three hydration operations. The variable n indicates the number of reaction stages, r refers to the particle size of the materials involved in the hydration retaliation t_0 signifies the end of the hydration induction period of the cement, and $t-t_0$ denotes the length of the accelerated period. Additionally, $F_1(\alpha)$, $F_2(\alpha)$, and $F_3(\alpha)$are the hydration reaction mechanism functions for the three processes, and $d\alpha/dt$ indicates the rate of the hydration reaction.

Employing the thermodynamic characteristics of hydration, the resultant α and Qmax are included into Eq. (3), and double logarithmic plots of ln[-ln(1-α)] and ln(t-t0) were generated. The hydration kinetic parameters n and K_1' for the NG stage of cement hydration can be ascertained by the analysis of linear regression. For stages I and D, the hydration kinetic equations are linear, allowing the same approach to be employed to derive the hydration kinetic parameters K_2' and K_3' for both stages. The calculated values of these hydration kinetic parameters are presented in Table 4.

Table 4. Kinetic parameters of hydration for G and G-4TSL

Samples	n	K_1'	K_2'	K_3'	α_1	α_2	Hydration mechanism
G	1.35426	0.14384	0.01627	0.00544	0.1007	0.2724	NG-I-D
G-4TSL	1.26378	0.20366	0.02896	0.01516	0.2104	0.5240	NG-I-D

By including the hydrating kinetic constants from Table 4 within Equations (6) to (8), the hydration speed lines for the NG, I, and D phases of G and G-4TSL may be

obtained, as seen in Fig. 7. $F_{NG}(\alpha)$, $F_I(\alpha)$, and $F_D(\alpha)$ denote the hydration reaction rates in the NG, I, and D phases, respectively, intersecting at points α_1 and α_2. The segment from curve 0 to α_1 represents the NG stage of the cement hydration process, α_1 to α_2 denotes the I stage, and α_2 is the end of the curve indicates the D stage of the cement hydration cycle. The rate of the cement hydration process is determined by the slowest of its three stages. Thus, the transition from α_1 to α_2 to the end of the curve represents the total rate of the cement hydration process, corresponding with the reaction rate dα/dt curve as established by isothermal calorimetry. This indicates that the mechanism of the reaction that causes cement to hydrate adheres to the NG-I-D model, wherein the control transitions from crystal formation and development to a phase's borderline reaction, finally progressing to a diffusion-controlled process.

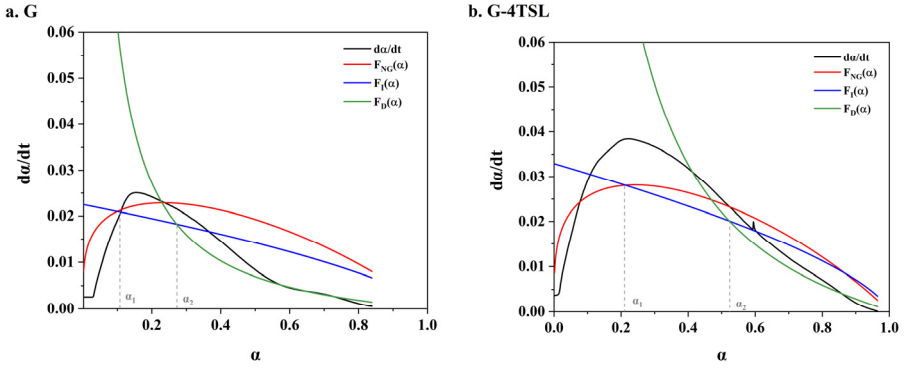

Fig. 7. Hydration rate profiles of G and G-4TSL at NG, I and D stages (a. Hydration rate profile of G at NG, I and D stages, b. Hydration rate profile of G-4TSL at NG, I and D stages

The value of α_1 at the NG stage of cement hydration rose from 0.1007 to 0.2104 with the addition of TSL, indicating an enhanced degree of hydration for G-4TSL at the NG stage compared to G, hence improving the hydration impact at this stage. The augmentation of the distance between the two sites α_1 and α_2 signifies that the proportion of the I control process within the entire cement hydration phase escalates following the integration of TSL, hence enhancing the hydration impact of the I stage. In stage D, the α_2 value of G-4TSL rose by 92.36 % relative to G, signifying that the inclusion of TSL enhanced the hydration impact in stage D.

The incorporation of TSL improved the whole hydration of the cement reaction process. The inclusion of TSL affected the procedure of hydration throughout the initial reaction phase, the induction phase, and the accelerated phase of cement hydration. This was demonstrated by the suppression of rapid hydration product formation in the initial reaction phase, a decrease in the length of the induction period, an augmentation of the hydration reaction during the accelerated phase, and an elevation in the cumulative exothermic heat of cement hydration. Furthermore, it enhanced the hydration reaction during the accelerated phase and increased the total exothermic heat in the initial hydration stage of Class G oil well cement, thereby promoting the early hydration reaction and demonstrating that TSL incorporation influenced both the microstructure of the cement pastes and the products of hydration.

3.3 Hydration Mechanism Analysis

Fig. 8 depicts TSL's function in promoting the hydration process of G at low temperatures. During the initial reaction phase, the presence of highly polarized Li^+ in the cement slurry accelerates the deterioration of the protective film formed by the initial hydration products on the surfaces of cement particles, thereby enhancing the interaction between cement particles and water and enabling the continuation of the hydration reaction. In the intermediate period of the reaction (i.e., 24-48 hours, corresponding to the accelerated phase of G and both the accelerated and decelerated phases of G-4TSL), the increase in the degree of hydration reaction attributable to the incorporation of TSL is negligible. This results from the rupture of the protective hydration layer on the surface of cement particles devoid of TSL, which also promotes the acceleration of their hydration process. During the deceleration phase of cement hydration, the production of additional CH prompts the reaction of Li^+ in TSL with OH^- in the liquid phase, yielding significant amounts of LiOH. This action subsequently increases the alkalinity of the liquid phase, hence enhancing the pace of cement hydration.

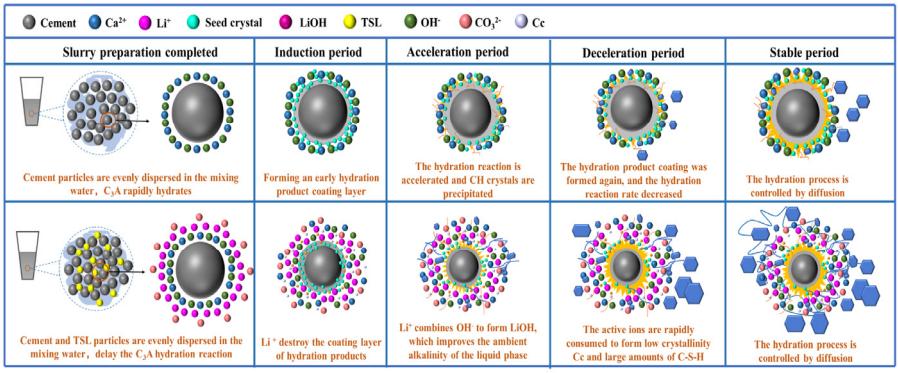

Fig. 8. Mechanism of action of TSL enhanced Class G oil well cement mechanical properties

3.4 Compressive Strength of Cement Pastes

Fig. 9 demonstrates the effect of different TSL doses on the compressive property of cement pastes, indicating an initial rise in strength then an increase in weakness with TSL incorporation. At TSL doses of 2 %-7 %, the compressive strength of cement pastes after 48 hours of curing surpassed 7.0 MPa, hence meeting the criteria for cementing construction [36]. At a TSL dose of 4 %, the cement pastes exhibited elevated compressive strength throughout all curing durations. The compressive strength of G-4TSL was 14.49 ± 0.31 MPa after curing at 4 °C for 48 hours, representing an increase of 455.17 % compared to G. Following a 72-hour curing period, the initial compressive strength of G-4TSL was measured at 15.74 ± 0.25 MPa, indicating a 280.19 % enhancement relative to G. This occurs because, at low dosages, TSL can interact with calcium hydroxide (CH) generated during cement hydration to produce lithium hydroxide (LiOH), which elevates the alkalinity in the liquid phase reaction within the cement, thus facilitating the dissolution of the aluminum phase and expediting the formation of

ettringite (AFt) [30]. Excessive TSL dose results in just a portion being soluble for the reaction, while the remainder may induce cracks and voids in the cement paste, hence diminishing compressive strength. It is noteworthy that cement pastes cured for 24 hours exhibited no compressive strength at any dosage; however, the experiment revealed that these pastes were molded. This phenomenon may be attributed to the initial cement particles being enveloped by a fragile layer of hydration products, where the hydration reaction relies on facile diffusion, resulting in a protracted strength development [37].

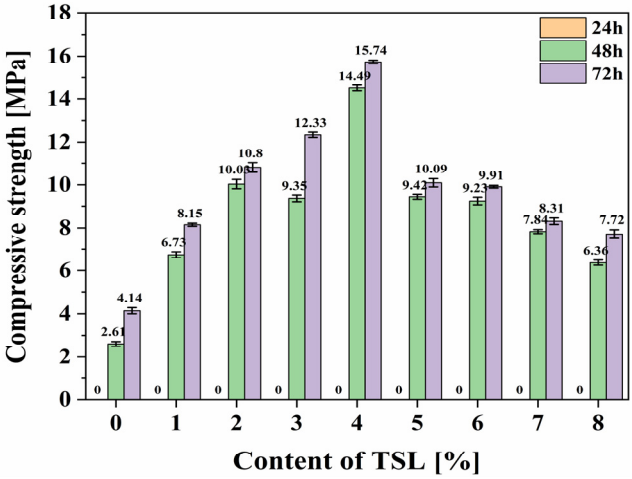

Fig. 9. Compressive strength of cement pastes with different TSL dosage

3.5 Physical Analysis of Cement Pastes

T The impact of TSL on the hydration products of class G oil well cement was examined by analyzing the crystalline and gel phases of G and G-4TSL cured for 24, 48, and 72 hours, utilizing a combination of XRD and thermogravimetric analysis, with the experimental findings presented in Figs. 10, 11, and 12. Figure 10 illustrates that the predominant crystalline phases of cement pastes cured at 4 °C are CH (PDF#04-0733, PDF#44-1481), AFt (PDF#41-1451), C_3S (PDF#49-0422), and C_2S (PDF#24-0034), with CH and AFt being hydration products, while C_3S and C_2S are mineral phases of the incompletely reacted cement. As curing age progressed, the intensity of the C_3S diffraction peak in the cement paste diminished, whereas the intensity of the C_2S diffraction peak exhibited minimal variation, suggesting that the hydration reaction of C_3S predominantly occurred during the first phase of cement hydration. The diffraction peak intensities of C_3S were significantly lower than those of G at all curing ages following the addition of 4 % TSL, suggesting that TSL facilitates the acceleration of the hydration process of C_3S. Moreover, the comparison of diffraction peak intensities revealed that the incorporation of TSL diminished the crystallinity of CH while enhancing the crystallinity of AFt. The Li^+ ions in TSL react with CH to produce LiOH, hence enhancing the alkalinity of the cement's liquid phase reaction and facilitating the acceleration of the cement hydration process [38].

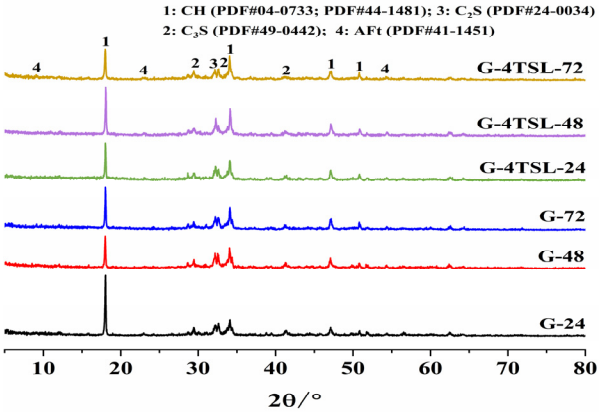

Fig. 10. XRD diffraction patterns of G and G-4TSL at various ages of cured

The XRD analysis revealed that the incorporation of TSL promoted the crystallization of AFt. Nevertheless, the effect of TSL on the gel products that hydrate remained unclear, and the XRD analysis was restricted to qualitative or semi-quantitative evaluations. Thus, the effect of TSL on the gel phases of cement hydration products was analyzed using thermogravimetric analysis, and the amounts of chemical bonded water and free calcium hydroxide in the cement were quantified. The chemically attached water content of the cement specimens may be ascertained using Eq. (9) proposed by Bhatty, whereas the free calcium hydroxide concentration can be calculated using Eq. (10) [39].

$$W_B = W_{dH} + W_{dOH} + 0.41 W_{dC} \tag{9}$$

$$W_{f\text{-}CH} = 4.11 \times W_{dOH} + 1.68 \times W_{dC} \tag{10}$$

W_B signifies the quantity of chemically bonded water, whereas W_{dH}, W_{dOH}, and W_{dC} indicate the relative loss of mass attributable to dehydration as well dehydroxylation, and decarbonization. The number 0.41, proposed by Rivera [40], denotes the ratio of the molecular weight of H_2O to that of CO_2 and functions as a conversion factor for determining the amount of chemically bonded water in calcium carbonate (Cc).

Figs. 11 and 12 depict the thermogravimetric analyses of G and G-4TSL cured at 4 °C for periods of 24, 48, and 72 hours, respectively. As temperatures increases form 40 °C to 1000 °C, the cement pastes undergo four unique stages of weight decrease [41], which are as follows: The initial phase occurs at 40~105 °C, signifying the evaporation or weight loss of unbound water in the cement pastes; the subsequent phase spans 105~420 °C, indicating the weight loss of bound water in the hydration products of C-S-H, AFt, and AFm in the cement pastes; the third phase, from 420~520 °C, relates to the weight loss from the decomposition products of CH in the cement pastes; the final phase, ranging from 520~950 °C, primarily corresponds to the weight reduction of CO_2 released from the dissolution of Cc. At 0 % doping of TSL, the weight loss is further delineated into two phases: 520~720 °C, corresponding to the decomposition of

low crystallinity Cc (Lc-Cc), and 720~950 °C, associated with the decomposition of high crystallinity Cc (Hc-Cc).

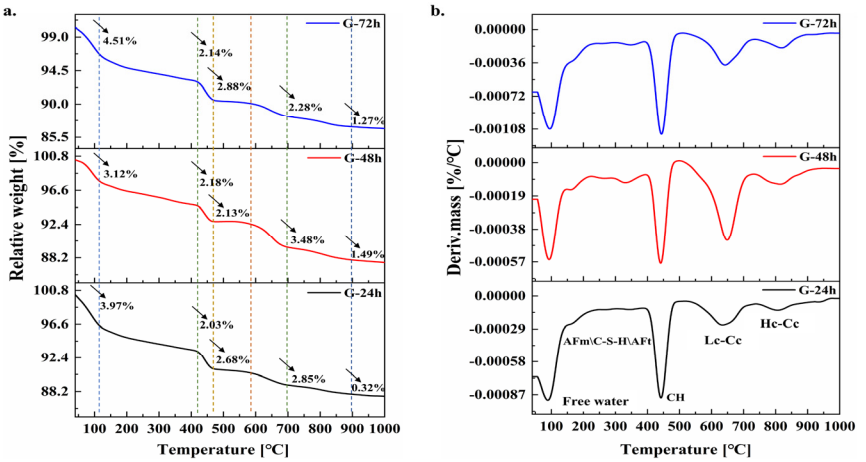

Fig. 11. TG/DTG curves of G (a.TG curve, b. DTG curve)

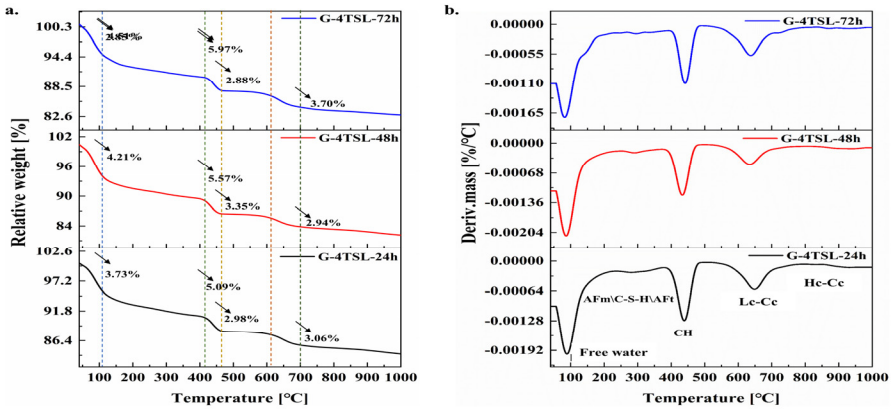

Fig. 12. TG/DTG curves of G-4TSL (a.TG curve, b. DTG curve)

The amount of bound chemically water and free calcium hydroxide present in the cement at each curing age may be estimated using Equations (9) and (10), as shown in Table 5. Table 5 demonstrates that as curing time increases, the water that is chemically bound content of the products of hydration in the cement paste specimens escalates, indicating a heightened degree of cement reaction of hydration and an increase in the volume of hydration products. Compared to G, the chemically bound water content of the hydration products of G-4TSL was increased at all curing periods. Following 24 hours of curing, the chemically bound water content of G hydration products was 6.01 %, whereas that of G-4TSL hydration products was 9.32 %, indicating a 55.07 %

increase relative to G. Following 48 hours of curing, the chemically bound water content of G hydration products was 6.35 %, reflecting a 5.66 % increase compared to G. The chemically bound water content of the hydration products of G-4TSL was 10.13 %, indicating an increase of 8.69 % relative to G-4TSL cured for 24 hours and 59.53 % compared to G cured for 48 hours. Following 72 hours of curing, the chemically bonded water content of the hydration products of G was 6.48 %, indicating an increase of 2.05 % relative to G cured for 48 hours. The chemically bonded water content of the hydration products of G-4TSL was 10.37 %, indicating an increase of 2.37 %. Compared with curing 72 h, the G was increased by 60.03 %. Analyzing the growth rates of chemically bound water content in the hydration products of G and G-4TSL indicates that the incorporation of TSL increases the chemically bound water content of the cement hydration products, hence promoting the overall hydration reaction of the cement.

Table 5. WB and f-CH content of G and G-4TSL at different curing ages

	G-24h	G-48h	G-72h	G-4TSL-24h	G-4TSL-48h	G-4TSL-72h
WB	6.01	6.35	6.48	9.32	10.13	10.37
f-CH	16.34	17.10	17.80	17.39	18.71	18.05

The variation in f-CH concentration among the hydration products of G and G-4TSL at all curing ages corresponded with the chemically bound water content. The f-CH concentration in the hydration products of G-4TSL exceeded that of G at all curing ages. After 24 hours of curing, the f-CH concentration in G-4TSL rose by 6.43 % relative to G. After a 48-hour cure, the f-CH concentration in G-4TSL rose by 9.42 % relative to G. After a 72-hour cure, the f-CH concentration in G-4TSL rose by 1.40 % relative to G. The augmentation of f-CH in the hydration products of class G oil well cements by TSL diminishes progressively with extended hydration time, attributable to the consumption of f-CH by Li^+ in the liquid phase, resulting in the formation of LiOH with elevated alkalinity. This process enhances the alkalinity of the cement's liquid phase and promotes the hydration reaction of the cement. The quantity of f-CH in the hydration products of G-4TSL is comparable to that in the hydration products of G throughout all hydration ages; however, the quantity of chemically bound water in the hydration products of G-4TSL is significantly greater.

3.6 Micro-Morphology of Cement Pastes

After 24, 48, and 72 hours of curing at 4 °C, the microscopic morphology of cement pastes with 0 % and 4 % TSL doping (designated as G and G-4TSL) was examined using a scanning electron microscope. The microscopic morphology and hydration products of cement pastes at varying curing durations are illustrated in Fig. 13, Fig. 14, and Fig. 15, respectively. Following 24 hours of curing, the cement matrix in G exhibited a somewhat loose composition, characterized by agglomerated flocculated hydration products C-S-H, with a minor presence of needle-like hydration products AFt, as seen in Fig. 13a. Following the incorporation of 4 % TSL, the cement paste exhibited

increased density, with a substantial quantity of gel-like hydration products, C-S-H, occupying the pores. The AFt underwent a transformation from acicular to columnar, whereas additional acicular AFt was generated. Furthermore, hexagonal sheets of CH may be detected interspersed among the hydration products, as illustrated in Fig. 13b. After 48 hours of curing, the structural densities of G were enhanced, resulting in the formation of substantial quantities of C-S-H and CH. The AFt underwent a transformation from needle-like structures to columnar forms; however, the C-S-H remained primarily as agglomerated flocs, while the CH appeared as thin flakes with a disordered and chaotic distribution [42]. Conversely, the C-S-H in the 4 % TSL doped cement paste exhibited a dense spatial network, with the columnar AFt equally distributed inside the C-S-H gel network, as seen in Figure 14. After 72 hours of curing, the C-S-H in G is present as both a spatial network and agglomerated flocculant; however, the network C-S-H is less dense, CH develops in plate-like structures, and AFt has completely converted into columns that are firmly attached to C-S-H. Conversely, following the incorporation of 4 % TSL, a significant quantity of coarse fibrous C-S-H, columnar AFt, and thick platelike CH was distinctly seen in the cement paste. Furthermore, the larger pores in the cement paste were entirely occupied by hydration products, converting into gel pores. The ordering of CH was enhanced, and the orthogonally staggered microcracks of the coarse fiber packing were observable, which improves the cohesive bond among the cement hydration products, as illustrated in Fig. 15.

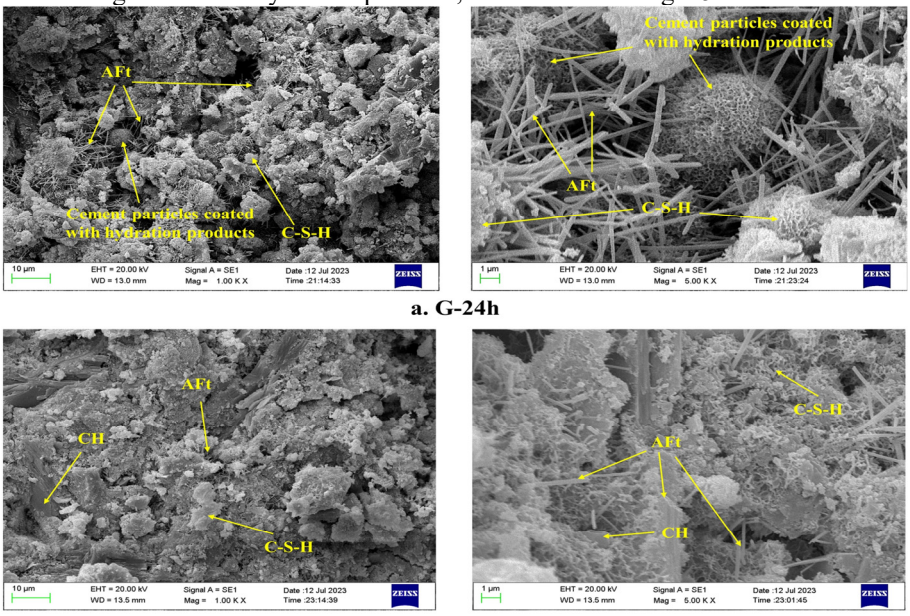

Fig. 13. Microscopic morphology of cement pastes cured at 4 °C for 24 h

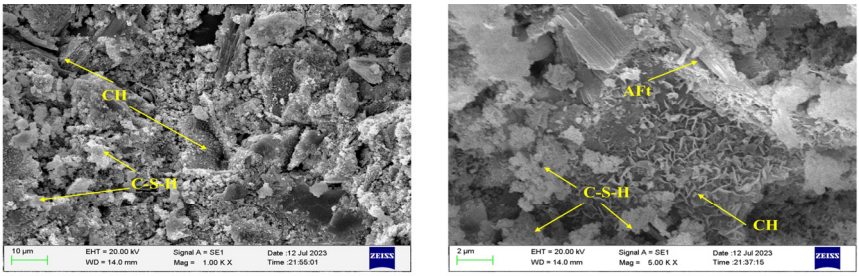

a. G-48h

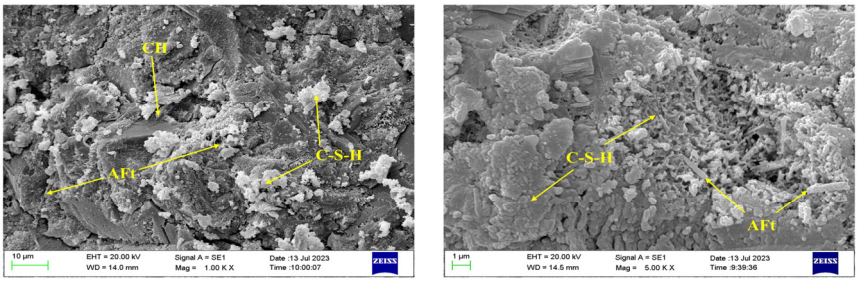

b. G-4TSL-48h

Fig. 14. Microscopic morphology of cement pastes cured at 4 °C for 48 h

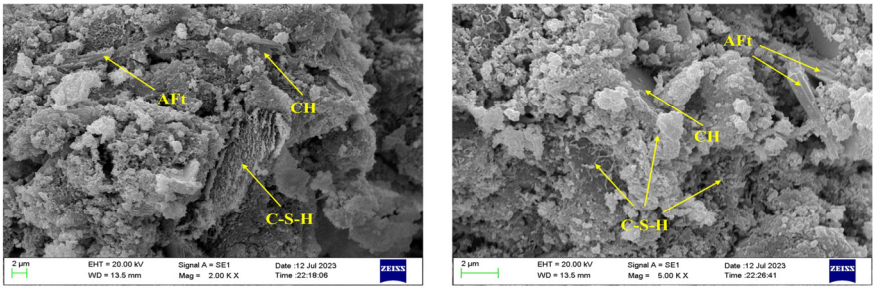

a. G-72h

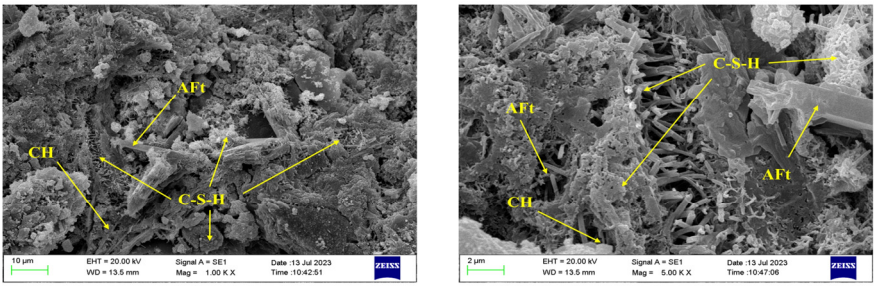

b. G-4TSL-72h

Fig. 15. Microscopic morphology of cement pastes cured at 4 °C for 72 h

The aforementioned micromorphological studies indicate that the inclusion of TSL can stimulate the creation and proliferation of cement hydration products AFt and CH,

hence enhancing the cement hydration process. The integration of TSL facilitates the organization of cement hydration products, enhances the transition of C-S-H from group flocculation to spatial reticulation, and aids in structural densification, thereby improving the compressive strength of cement pastes.

4 Conclusion

This study investigates the insufficient or halted hydration of cement in deep water, ultra-deep water, and polar cold sea environments, particularly concerning low-temperature strength development. It explores the impact of alkali metal salt TSL on the hydration of G. Following experimental research and analysis, the study reaches the subsequent conclusions:

(1) The addition of 4 % TSL primarily increases the heat release during both the accelerated and decelerated stages of G hydration, while decreasing the overall cumulative heat release by 8.93 % over 168 hours.

(2) The hydration mechanism of TSL combined with G remains NG-I-D; however, TSL amplifies the hydration effects during the NG, I, and D stages of G hydration.

(3) TSL may significantly enhance the compressive strength of cement pastes. At a dose of 4 %, the compressive strength reaches its peak, measuring 14.49 ± 0.31 MPa after 48 hours, therefore satisfying the cementing requirements.

(4) TSL enhances the hydration of cement, creates a protective layer of low-crystallinity Cc hydration products, encourages the ordered growth of AFt and CH, aids in the transformation of C-S-H gel from agglomerated flocculent to a spatial lattice, and facilitates the densification of C-S-H.

Acknowledgements

The authors express gratitude for the funding from the Natural Science Foundation of the Science and Technology Department of Sichuan Province (2024NSFSC0154). The authors express gratitude to Petrochina Southwest Oil and Gas Field Company Development Division, Advanced Cementing Materials Research Center of Southwest Petroleum University, and the School of New Energy and Materials of Southwest Petroleum University for their generous support in laboratory testing.

Reference

1. G. Yang, T. Liu, B.P. Aleksandravih, Y. Wang, Y. Feng, D. Wen, C. Fang, Temperature regulation effect of low melting point phase change microcapsules for cement slurry in nature gas hydrate-bearing sediments, Energy. 253 (2022) 124115. https://doi.org/10.1016/j.energy.2022.124115.
2. Y. Bu, W. Du, J. Du, A. Zhou, C. Lu, H. Liu, S. Guo, The potential utilization of lecithin as natural gas hydrate decomposition inhibitor in oil well cement at low temperatures, Constr. Build. Mater. 269 (2021) 121274. https://doi.org/10.1016/j.conbuildmat.2020.121274.

3. M. Huo, H. Liu, Y. Bu, R. Ma, H. Xu, J. Du, X. Pang, A. Zhou, C. Ma, Effect of main functional groups of cement slurry additives on the stability of methane hydrate: Experiment and molecular dynamics simulation, Geoenergy Sci. Eng. 228 (2023) 212024. https://doi.org/10.1016/j.geoen.2023.212024.
4. Q. Feng, Y. Zhang, Z. Peng, Y. Zheng, X. Chen, Preparation and investigation of microencapsulated thermal control material used for the cementing of gas hydrate formations, Colloids Surfaces A Physicochem. Eng. Asp. 648 (2022) 129182. https://doi.org/10.1016/j.colsurfa.2022.129182.
5. J. Li, C. Zhang, Z. Wu, G. Zhang, Q. Gao, K. Liu, X. Cheng, Can low hydration heat cement prevent the decomposition of natural gas hydrate under high pressure and low temperature?, J. Nat. Gas Sci. Eng. 97 (2022) 104347. https://doi.org/10.1016/j.jngse.2021.104347.
6. F. Xi, F. Sun, J. Wang, K. Yang, Optimization design and performance evaluation of new type low temperature early strength cement slurry, Proc. Int. Offshore Polar Eng. Conf. 2020-Octob (2020) 1138–1141.
7. C. Wang, X. Chen, R. Wang, Study on the performance and mechanism of accelerators LSA-1 and LSA-2 for deepwater well cementing at low temperatures, J. Nat. Gas Sci. Eng. 32 (2016) 150–157. https://doi.org/10.1016/j.jngse.2016.03.087.
8. S. Hancock, G. Moridis, S. Wilson, A. Robertson, Well design requirements for deepwater and arctic onshore gas hydrate production wells, Proc. Annu. Offshore Technol. Conf. 4 (2010) 3232–3238. https://doi.org/10.4043/21015-ms.
9. P.E. Conference, G. Drilling, C. Technology, Cement Slurry for Oil and Gas Wells in Polar Alpine Region, (2023) 100–103.
10. S. Mozaffari, O. Rahmani, A. Piroozian, Z. Ziabakhsh-Ganji, H. Mostafavi, Oil-well lightweight cement slurry for improving compressive strength and hydration rate in low-temperature conditions, Constr. Build. Mater. 357 (2022) 129301. https://doi.org/10.1016/j.conbuildmat.2022.129301.
11. J. Cai, C. Zhang, L. Zeng, H. Xu, J. Wang, K. Liu, X. Cheng, Preparation and action mechanism of temperature control materials for low-temperature cement, Constr. Build. Mater. 312 (2021) 125364. https://doi.org/10.1016/j.conbuildmat.2021.125364.
12. X. Zeng, C. Ma, G. Long, H. Dang, Y. Xie, Hydration kinetics of cement composites with different admixtures at low temperatures, Constr. Build. Mater. 225 (2019) 223–233. https://doi.org/10.1016/j.conbuildmat.2019.07.153.
13. C. Wang, W. Xiang, J. Du, X. Yao, Heat flow inhibitor suitable for oil well cement at low temperature, Constr. Build. Mater. 329 (2022) 127105. https://doi.org/10.1016/j.conbuildmat.2022.127105.
14. Y. Xu, T. He, R. Yang, X. Ma, New insights into the impact of inorganic salt on cement pastes mixed with alkali free liquid accelerator in low temperature, J. Build. Eng. 70 (2023) 106419. https://doi.org/10.1016/j.jobe.2023.106419.
15. J. Liu, L. Zhao, L. Chi, G. Luo, T. Li, S. Cai, Effect of multilayer graphene oxide on the hydration and early mechanical strength of cement mortar in low temperature, Constr. Build. Mater. 364 (2023) 129997. https://doi.org/10.1016/j.conbuildmat.2022.129997.
16. H. Wei, S. Zhou, The use of liquid nano-silica in cementing work and its advantages for cement sheath integrity, 55th U.S. Rock Mech. / Geomech. Symp. 2021. 5 (2021).
17. C. Wang, X. Chen, R. Wang, Do chlorides qualify as accelerators for the cement of deepwater oil wells at low temperature?, Constr. Build. Mater. 133 (2017) 482–494. https://doi.org/10.1016/j.conbuildmat.2016.12.089.
18. T. Chen, B. Ren, Z. Wang, X. Meng, Y. Ning, Y. Lv, Effect of early strength agent on the hydration of geopolymer mortar at low temperatures, Case Stud. Constr. Mater. 17 (2022) e01419. https://doi.org/10.1016/j.cscm.2022.e01419.

19. J. Yun, C. Zhao, X. Li, W. Zhang, H. Liu, B. Liu, Rheological properties and early mechanical strength of oil-well cement modified by hybrid nano-silica and nano-hexagonal boron nitride, Constr. Build. Mater. 356 (2022) 129291. https://doi.org/10.1016/j.conbuildmat.2022.129291.
20. M.T. Maagi, G. Jun, Effect of the particle size of nanosilica on early age compressive strength in oil-well cement paste, Constr. Build. Mater. 262 (2020) 120393. https://doi.org/10.1016/j.conbuildmat.2020.120393.
21. H. Zhou, X. Qi, C. Ma, Z. Fang, J. Lou, H. Chen, X. Guo, Effect and mechanism of composite early-strength agents on sulfoaluminate cement-based UHPC, Case Stud. Constr. Mater. 18 (2023) e01768. https://doi.org/10.1016/j.cscm.2022.e01768.
22. G. Ren, Z. Tian, J. Wu, X. Gao, Effects of combined accelerating admixtures on mechanical strength and microstructure of cement mortar, Constr. Build. Mater. 304 (2021) 124642. https://doi.org/10.1016/j.conbuildmat.2021.124642.
23. N. Cristelo, I. Garcia-Lodeiro, J.F. Rivera, T. Miranda, Á. Palomo, J. Coelho, A. Fernández-Jiménez, One-part hybrid cements from fly ash and electric arc furnace slag activated by sodium sulphate or sodium chloride, J. Build. Eng. 44 (2021). https://doi.org/10.1016/j.jobe.2021.103298.
24. S. Zhang, Y. Zhao, H. Ding, J. Qiu, C. Hou, Effect of sodium chloride concentration and pre-curing time on the properties of cemented paste backfill in a sub-zero environment, J. Clean. Prod. 283 (2021) 125310. https://doi.org/10.1016/j.jclepro.2020.125310.
25. Z. Shi, C. Shi, H. Liu, P. Li, Effects of triisopropanol amine, sodium chloride and limestone on the compressive strength and hydration of Portland cement, Constr. Build. Mater. 125 (2016) 210–218. https://doi.org/10.1016/j.conbuildmat.2016.08.030.
26. X. Pang, P. Boul, W. Cuello Jimenez, Isothermal calorimetry study of the effect of chloride accelerators on the hydration kinetics of oil well cement, Constr. Build. Mater. 77 (2015) 260–269. https://doi.org/10.1016/j.conbuildmat.2014.12.077.
27. M. Niziurska, J. Małolepszy, G. Malata, The influence of lithium carbonate on phase composition of calcium aluminate cement paste, Procedia Eng. 108 (2015) 363–370. https://doi.org/10.1016/j.proeng.2015.06.159.
28. X. Ben, L. Jiang, M.Z. Guo, W. Jin, L. Chen, F. Zhi, S. Gao, K. Xia, Effect of lithium citrate on hydration of cement paste, J. Build. Eng. 52 (2022) 104425. https://doi.org/10.1016/j.jobe.2022.104425.
29. L. Sheng, X. Wang, L. Wang, J. Wang, H. Xu, X. He, In-situ polymerized separator enables propylene carbonate electrolyte compatible with high-performance lithium batteries, J. Power Sources. 551 (2022) 232172. https://doi.org/10.1016/j.jpowsour.2022.232172.
30. Y. Zhang, Y. Wang, T. Li, Z. Xiong, Y. Sun, Effects of lithium carbonate on performances of sulphoaluminate cement-based dual liquid high water material and its mechanisms, Constr. Build. Mater. 161 (2018) 374–380. https://doi.org/10.1016/j.conbuildmat.2017.11.130.
31. American Petroleum Institute, API RP 10B-2, Recommended practice for testing well cements, 2013, P.124, (n.d.).
32. H.M. Yang, S.M. Zhang, L. Wang, P. Chen, D.K. Shao, S.W. Tang, J.Z. Li, High-ferrite Portland cement with slag: Hydration, microstructure, and resistance to sulfate attack at elevated temperature, Cem. Concr. Compos. 130 (2022). https://doi.org/10.1016/j.cemconcomp.2022.104560.
33. X. Lyu, G. Yao, Z. Wang, Q. Wang, L. Li, Hydration kinetics and properties of cement blended with mechanically activated gold mine tailings, Thermochim. Acta. 683 (2020) 178457. https://doi.org/10.1016/j.tca.2019.178457.
34. R. Krstulović, P. Dabić, A conceptual model of the cement hydration process, Cem. Concr. Res. 30 (2000) 693–698. https://doi.org/10.1016/S0008-8846(00)00231-3.

35. Y. Su, H. Zhao, X. He, Z. Zheng, Q. Ma, J. Ding, M. Bao, The effect of wet-grinding phosphorus slag on the hydration kinetics of Portland cement, Constr. Build. Mater. 364 (2023) 129942. https://doi.org/10.1016/j.conbuildmat.2022.129942.
36. J. Cai, J. Zhou, C. Liu, K. Mei, C. Zhang, X. Cheng, Microencapsulated phase change material-cement composites for cementing the natural gas hydrate layer, Constr. Build. Mater. 399 (2023) 132591. https://doi.org/10.1016/j.conbuildmat.2023.132591.
37. Y. Zhou, Y. Yan, Y. Qin, C. Yu, W. Wang, J. Liu, K. Wang, The effect of temperature rise inhibitor on the hydration and strength development of slag/fly ash blended cement paste, Constr. Build. Mater. 395 (2023) 132307. https://doi.org/10.1016/j.conbuildmat.2023.132307.
38. H. Tan, M. Li, X. He, Y. Su, J. Zhang, H. Pan, J. Yang, Y. Wang, Preparation for microlithium slag via wet grinding and its application as accelerator in Portland cement, J. Clean. Prod. 250 (2020) 119528. https://doi.org/10.1016/j.jclepro.2019.119528.
39. J.I. Bhatty, Hydration Versus Strength in a Portland, 106 (1986) 93–103.
40. J. Rivera Lozano, La hidratación de la pasta de cemento con adiciones activas, Tesis Doctoral Facultad de Ciencias, Universidad Autónoma de Madrid, 2004., (2008) 1–14.
41. C. Zhang, J. Cai, H. Xu, X. Cheng, X. Guo, Mechanical properties and mechanism of wollastonite fibers reinforced oil well cement, Constr. Build. Mater. 260 (2020) 120461. https://doi.org/10.1016/j.conbuildmat.2020.120461.
42. C. Zhang, J. Cai, X. Cheng, X. Zhang, X. Guo, Y. Li, Interface and crack propagation of cement-based composites with sulfonated asphalt and plasma-treated rock asphalt, Constr. Build. Mater. 242 (2020) 118161. https://doi.org/10.1016/j.conbuildmat.2020.118161.